Heliyon 10 (2024) e32294

Contents lists available at ScienceDirect

Heliyon

journal homepage: www.cell.com/heliyon

Research article

Development and evaluation of a disulfidoptosis-related lncRNA index for prognostication in clear cell renal cell carcinoma

Renhui Guan [a], You Zuo [b,c], Qinglong Du [b,c], Aijing Zhang [b,c], Yijian Wu [b,c], Jianguo Zheng [b,c], Tongrui Shi [b,c], Lin Wang [b,c], Hui Wang [b,d,**], Nengwang Yu [b,*]

[a] Clinical College, Chengde Medical University, Chengde, Hebei, 067000, China
[b] Department of Urology, Qilu Hospital of Shandong University, Jinan, Shandong, 250012, China
[c] Cheeloo College of Medicine, Shandong University, Jinan, Shandong, 250012, China
[d] Department of Urology, Qilu Hospital of Shandong University Dezhou Hospital, Dezhou, 253000, China

ARTICLE INFO

Keywords:
Clear cell renal cell carcinoma
Single-cell deconvolution
Disulfidoptosis
Long non-coding RNA
Prognostic index
Tumor microenvironmen

ABSTRACT

Background: This study introduces a novel prognostic tool, the Disulfidoptosis-Related lncRNA Index (DRLI), integrating the molecular signatures of disulfidoptosis and long non-coding RNAs (lncRNAs) with the cellular heterogeneity of the tumor microenvironment, to predict clinical outcomes in patients with clear cell renal cell carcinoma (ccRCC).

Methods: We analyzed 530 tumor and 72 normal samples from The Cancer Genome Atlas (TCGA), employing k-means clustering based on disulfidoptosis-associated gene expression to stratify ccRCC samples into prognostic groups. lncRNAs correlated with disulfidoptosis were identified and used to construct the DRLI, which was validated by Kaplan-Meier and receiver operating characteristic curves. We utilized single-cell deconvolution analysis to estimate the proportion of immune cell types within the tumor microenvironment, while the ESTIMATE and TIDE algorithms were employed to assess immune infiltration and potential response to immunotherapy.

Results: The Disulfidoptosis-Related lncRNA Index (DRLI) effectively stratified ccRCC patients into high and low-risk groups, significantly impacting survival outcomes ($P < 0.001$). High-risk patients, marked by a unique lncRNA profile associated with disulfidoptosis, faced worse prognoses. Single-cell analysis revealed marked tumor microenvironment heterogeneity, especially in immune cell makeup, correlating with patient risk levels. In prognostic predictions, DRLI outperformed traditional clinical indicators, achieving AUC values of 0.779, 0.757, and 0.779 for 1-year, 3-year, and 5-year survival in the training set, and 0.746, 0.734, and 0.750 in the validation set. Notably, while the constructed nomogram showed exceptional predictive capability for short-term prognosis (AUC = 0.877), the DRLI displayed remarkable long-term predictive accuracy, with its AUC value reaching 0.823 for 10-year survival, closely approaching the nomogram's performance.

Conclusions: The study introduces the DRLI as a groundbreaking molecular stratification tool for ccRCC, enhancing prognostic precision and potentially guiding personalized treatment strategies. This advancement is particularly significant in the context of long-term survival predictions. Our findings also elucidate the complex interplay between disulfidoptosis, lncRNAs, and the immune microenvironment in ccRCC, offering a comprehensive perspective on its pathogenesis and

* Corresponding author. Department of Urology, Qilu Hospital of Shandong University, Jinan, Shandong, 250012, China.
** Corresponding author. Department of Urology, Qilu Hospital of Shandong University, Jinan, Shandong, 250012, China.
E-mail addresses: aaahuiwang@163.com (H. Wang), qiluyunengwang@hotmail.com (N. Yu).

https://doi.org/10.1016/j.heliyon.2024.e32294
Received 31 January 2024; Received in revised form 22 May 2024; Accepted 31 May 2024
Available online 3 June 2024

progression. The DRLI and the nomogram together represent significant strides in ccRCC research, highlighting the importance of molecular-based assessments in predicting patient outcomes.

Abbreviations

ccRCC	Clear Cell Renal Cell Carcinoma
DRLI	Disulfidoptosis-Related lncRNA Index
TCGA	The Cancer Genome Atlas
lncRNAs	Long Non-Coding RNAs
KM	Kaplan-Meier
ROC	Receiver Operating Characteristic
AUC	Area Under the Curve
ESTIMATE	Estimation of STromal and Immune cells in MAlignant Tumor tissues using Expression data
TIDE	Tumor Immune Dysfunction and Exclusion
PCA	Principal Component Analysis
GSVA	Gene Set Variation Analysis
KEGG	Kyoto Encyclopedia of Genes and Genomes
GO	Gene Ontology
HR	Hazard Ratio
TMB	Tumor Mutation Burden
UISS	University of California, Los Angeles Integrated Staging System

1. Background

Renal cell carcinoma (RCC), with clear cell renal cell carcinoma (ccRCC) as its major subtype, represents about 4 % of all malignancies, contributing to the increasing global burden with approximately 180,000 deaths annually [1]. The biological behavior and clinical outcomes of RCC are remarkably diverse. A significant number of smaller, non-aggressive renal tumors remain undetected due to their asymptomatic nature [2,3], yet up to 30 % of patients experience recurrence or metastasis post-surgery, adversely affecting their prognosis [4].

There is a crucial need to develop a more accurate risk stratification system for RCC to inform and optimize treatment strategies. The current international standard for RCC staging is the TNM system by the American Joint Committee on Cancer (AJCC), which considers tumor size, local invasion, lymph node involvement, and distant metastasis. Despite its widespread use and iterative updates, the TNM system provides only a snapshot of the tumor's cross-sectional status at diagnosis and fails to capture the longitudinal and biological aggression of the cancer [5,6]. Similarly, the University of California, Los Angeles Integrated Staging System (UISS), and the Mayo Clinic's prognostic model, which includes renal cancer stage, size, grade, and necrosis, offer broader parameters but still insufficiently reflect the heterogeneity of kidney cancer, as indicated by their C-index scores in external validation [7–9]. These limitations underscore the demand for novel, more discriminating models for kidney cancer risk stratification.

Among the emerging frontiers in RCC research is the characterization of cell death modalities, particularly disulfidoptosis—a form of programmed cell death driven by disulfide stress, known for its pivotal role in the pathogenesis and progression of various cancers, including RCC [10–12]. This novel cell death process offers a promising target for therapeutic intervention and serves as a potential prognostic marker, especially when considered in conjunction with long non-coding RNAs (lncRNAs).

The intricate interplay between disulfidoptosis and lncRNAs has opened new avenues for constructing advanced prognostic models for ccRCC. By exploring disulfidoptosis-related lncRNAs, our study aims to build a prognostic model that transcends the capabilities of traditional clinical staging systems. This model endeavors to provide a more granular risk stratification by integrating molecular markers that reflect the underlying tumor biology more accurately.

Single-cell deconvolution offers a sophisticated lens to dissect the cellular heterogeneity inherent in ccRCC [13,14]. It allows for the detailed estimation of tumor cell composition, revealing the subtleties of the tumor microenvironment at a cellular level. This high-resolution mapping of cellular populations within the tumor milieu contributes significantly to the understanding of RCC's biological complexity.

Lastly, the immune microenvironment plays a crucial role in the progression and treatment responsiveness of ccRCC [15]. Our model incorporates the assessment of immune infiltration, providing insights into the interplay between the tumor and its immune landscape. This approach not only informs prognosis but also has the potential to guide immunotherapeutic strategies, offering a tailored approach to patient management.

Through this comprehensive methodology, combining the novel insights of disulfidoptosis with the regulatory landscape of lncRNAs, the precision of single-cell deconvolution, and the dynamics of the immune microenvironment, we aim to redefine the

prognostic framework for ccRCC. This integrative model is poised to enhance our ability to predict clinical outcomes and tailor therapeutic interventions, marking a significant advancement in the personalized care of RCC patients.

2. Methods

2.1. Study design and data acquisition

This study sourced omics data for differential comparison and predictive model construction from The Cancer Genome Atlas (TCGA) database. The "TCGAbiolinks" package in R was utilized to download renal clear cell carcinoma (ccRCC) data [16,17]. Transcripts for mRNA and lncRNA were identified according to GRCh38. p13 reference [18]. The publicly available data did not contain identifiable patient information, thereby negating the need for ethical review. Transcriptome data were matched with clinical information, excluding samples lacking any data type or duplicates.

2.2. Construction of the Disulfide Stress-Related Long Non-Coding RNA index (DRLI)

To construct the Disulfide Stress-Related Long Non-Coding RNA Index (DRLI), we first employed the Wilcoxon test to identify lncRNAs with significant expression differences between cancerous and normal tissues. These selected lncRNAs were then subjected to correlation analysis with disulfide stress-related genes, considering an absolute correlation coefficient greater than 0.3 and a p-value less than 0.001 as significant. The lncRNAs significantly associated with disulfide stress were combined with clinical data for univariate analysis. The prognostically significant lncRNAs were dimensionally reduced through Lasso regression, followed by the development of a prognostic model using multivariate Cox regression. Each sample's score was calculated according to the DRLI formula, stratifying patients into high and low-risk groups. The discriminative ability of DRLI was validated through Kaplan-Meier (KM) survival curves and receiver operating characteristic (ROC) curves.

2.3. Gene Set Variation Analysis (GSVA)

For Gene Set Variation Analysis (GSVA), we used the GSVA package [19] in R to calculate enrichment scores for each sample in predefined gene sets, following the method described by Hänzelmann et al. Additionally, the h. all.v7.4. symbols.gmt subset was downloaded from the Molecular Signatures Database (MSigDB) [20].

The Hallmark gene sets used in our GSVA analysis represent key pathways and states in cellular biology. These gene sets have been carefully curated for co-expression across multiple datasets to evaluate the activity of relevant pathways in the samples. By computing enrichment scores for each gene set per sample, we generated an enrichment score matrix to aid in identifying potential biological markers and therapeutic targets.

2.4. Single-cell transcriptome data

Single-cell sequencing data for ccRCC samples from three patients included in the study were obtained from the GSE222703 dataset [21], prepared using the Chromium 10× platform post-nephrectomy and sequenced on the Illumina NovaSeq 6000 system. Specifically, the analysis encompassed 27,963 cells from 3 ccRCC patients, with cell populations labeled as 23 distinct cell types. Clustering results were visualized using Uniform Manifold Approximation and Projection (UMAP) for dimension reduction [22].

2.5. Deconvolution of ccRCC bulk RNA-seq data

A comprehensive analysis of the tumor microenvironment was conducted utilizing two distinct reference gene sets for deconvolution, both implemented within the CIBERSORTx platform. Firstly, single-cell deconvolution was performed using the CIBERSORTx platform [14], with the log-normalized expression matrix of 10 major cell populations from the GSE222703 dataset [21], comprising 27,963 cells from ccRCC patients, serving as the basis for generating a signature matrix. This matrix was utilized as a reference to estimate the proportions of 23 cell types in the TCGA ccRCC cohort, incorporating 1000 permutations and S-mode batch correction.

In addition, an analysis of immune cell composition was conducted using the LM22 gene set [14], recognized for its reference to 22 immune cell types and implemented within the CIBERSORTx platform. Transcriptome data from ccRCC patients were input into CIBERSORTx and applied to the LM22 signature to quantify the relative abundance of immune cells. This secondary analysis provided complementary insights into the immune landscape within the tumor microenvironment.

2.6. Estimation of STromal and immune cells in MAlignant tumor tissues using expression data (ESTIMATE)

The ESTIMATE algorithm [23] was employed to gauge tumor purity and the presence and extent of infiltrating stromal and immune cells in tumor tissues. This algorithm, based on single-sample Gene Set Enrichment Analysis, yields three distinct scores: 'stromal score' indicating the stromal cell abundance, 'immune score' quantifying immune cell infiltration, and 'estimate score' inferring overall tumor purity. These scores collectively enhance our comprehension of the tumor microenvironment, employing gene expression data to decipher the intricate interplay between tumor cells, stromal cells, and immune infiltrates.

2.7. Tumor immune dysfunction and exclusion (TIDE)

The Tumor Immune Dysfunction and Exclusion (TIDE) scoring system [24,25] was used to predict tumor responsiveness to immune checkpoint blockade therapy. The TIDE algorithm assesses the likelihood of immune evasion from tumor gene expression data, indicating potential immunotherapy response. Scores obtained via the TIDE web tool from gene expression profiles were utilized to determine the efficacy of checkpoint inhibitors in treating these tumors, categorizing them based on their predicted response to immunotherapy.

2.8. Correlation analysis

Correlation analysis between gene expression levels was guided by data distribution. Pearson's correlation coefficient was implemented for normally distributed data to capture linear relationships, while Spearman's rank correlation was employed for non-normally distributed data, suitable for identifying monotonic relationships. The analysis set a stringent correlation threshold of 0.3 and a p-value threshold of 0.001 to ensure that only significant and relevant correlations were identified.

3. Results

3.1. Construction of mRNA clustering for disulfidptosis and Disulfidptosis-Related lncRNA index

We retrieved renal clear cell carcinoma data from the TCGA database, which consisted of 530 tumor samples and 72 normal samples for control. The workflow of our study is illustrated (Fig. 1). Accompanying clinical information and transcriptome expression data were downloaded, from which mRNA and lncRNA expression matrices were extracted according to GENCODE 2021 [18] guidelines. In a related study [10], we identified 10 genes associated with disulfidptosis. We applied k-means clustering for unsupervised classification of ccRCC samples into two distinct clusters, C1 and C2, as shown in the heatmap (Fig. 2A). Survival analysis revealed a significant prognostic difference between clusters C1 and C2, with C1 demonstrating a substantially better prognosis than C2 (Fig. 2B), signifying the relevance of disulfide-related genes to the prognosis of ccRCC patients. To further explore prognostic factors in ccRCC linked to the vital biological process of disulfidptosis, Spearman's correlation analysis was conducted to identify lncRNAs from the expression data that correlated with the 10-gene disulfidptosis set, yielding 174 disulfidptosis-associated lncRNAs (Fig. 2C). Subsequently, through univariate Cox regression, we screened lncRNAs impacting prognosis, followed by dimensionality reduction using Lasso (Fig. 2D), and ultimately constructed the DRLI using multivariate Cox regression. The DRLI is composed of 8 lncRNAs, with the calculation formula as follows: DRLI = 0.824336231 × AC073896.2–0.596657862 × AC005281.1 + 1.396867877 × ALMS1-IT1 + 0.911216855 × ARHGAP29-AS1 - 0.208127865 × LINC02747–0.353676173 × SPINT1-AS1 - 1.548271173 × SUCLG2-AS1 - 1.527521165 × ZRANB2-AS1, and the correlation of these 8 lncRNAs with the 10 disulfidoptosis genes is depicted in Fig. 2E.

3.2. Validation of the discriminatory ability of the DRLI

The median value of the Disulfidptosis-Related lncRNA Index (DRLI) was utilized as a cutoff to stratify patients in the training set

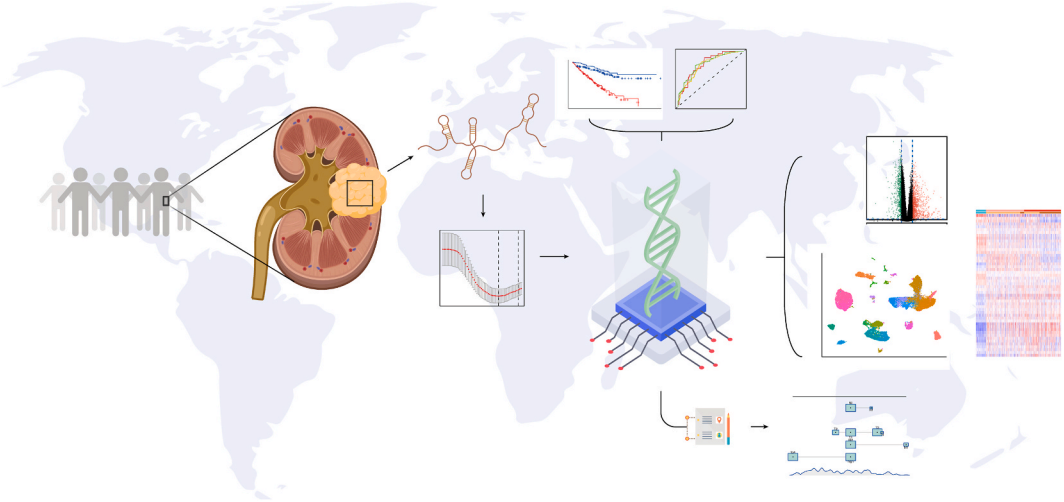

Fig. 1. Workflow:This figure illustrates the workflow of our study. Initially, clear cell renal cell carcinoma (ccRCC) data were obtained from The Cancer Genome Atlas (TCGA) database. Subsequently, utilizing disulfidoptosis-associated long non-coding RNAs (lncRNAs) identified from the tumor, we constructed the Disulfidoptosis-Related lncRNA Index (DRLI) using LASSO-Cox regression. Finally, we evaluated and validated the predictive capability of DRLI.

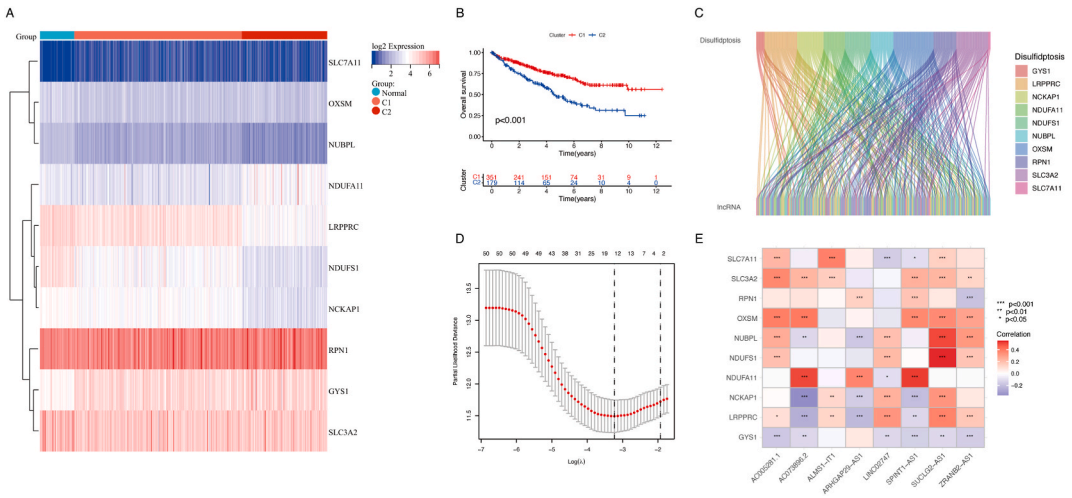

Fig. 2. A: Heatmap of k-means clustering in ccRCC samples based on disulfidoptosis-associated gene expression, dividing samples into two clusters, C1 and C2. B: Kaplan-Meier survival curves showing the prognostic differences between C1 and C2 clusters in ccRCC patients. C: Correlation heatmap of 174 disulfidoptosis-associated lncRNAs with the disulfidoptosis gene set in ccRCC. D: Lasso regression plot demonstrating dimensionality reduction in the selection of prognostic lncRNAs. E: Correlation matrix of the 8 lncRNAs constituting the DRLI and their associated disulfidoptosis genes.

into high and low-risk groups. A heatmap depicting the expression of the 8 lncRNAs in the TCGA-ccRCC cohort, along with Risk Score Plot and Survival Status Plot, are illustrated in Fig. 3A. Using the training set-derived DRLI formula and cutoff, stratification of the validation cohort was calculated. The OS survival curve (Kaplan-Meier) for the training set is presented in Fig. 3B. The PFS (Progression-Free Survival) Kaplan-Meier curves for the validation cohort confirmed that patients in the high-risk DRLI group had significantly worse survival outcomes compared to the low-risk group ($P < 0.001$) (Fig. 3C). In addition to the DRLI, we also analyzed the prognosis of the ccRCC cohort by combining the DRLI with the disulfidoptosis gene subtypes C1 and C2. Although the prognosis of subtype C2 was markedly worse than C1 (Fig. 2B), there was no significant difference in survival outcomes between the High + C2 group and High + C1 group, as well as between the Low + C2 and Low + C1 groups (Fig. 3D). This suggests that the impact of DRLI on prognosis supersedes the influence of disulfidoptosis gene subtype classification on the prognosis of ccRCC. ROC curves for both the training and validation cohorts demonstrated that the AUC values for 1-year, 3-year, and 5-year survival were 0.779, 0.757, and 0.779 for the training cohort (Figs. 3E), 0.746 and 0.734, and 0.750 for the validation cohort (Fig. 3F), respectively. Our DRLI effectively predicts patient prognosis in ccRCC, with comparable efficacy in both training and validation cohorts, indicating a well-fitted model. The predictive accuracy of DRLI, age, gender, and tumor staging parameters (T, N, M) for patient survival was assessed over time through the C-index, with DRLI outperforming other clinical indicators (Fig. 3G).

3.3. Construction of the nomogram

Single and multivariate Cox regression analyses were conducted to evaluate the impact of clinical information and the risk model on prognosis. Results indicated that T stage, N stage, M stage, age, and DRLI were all risk factors affecting the prognosis of ccRCC (Fig. 4A), with all but N stage serving as independent risk factors. DRLI, in particular, exhibited a hazard ratio (HR) of 2.996 (95 % CI: 1.790–4.916) (Fig. 4B). A nomogram incorporating T stage, N stage, M stage, age, and DRLI was constructed using 'regplot' and 'rms' package approaches in Cox regression (Fig. 4C). The nomogram demonstrated good predictive ability with a C-index of 0.798 (95 % CI: 0.757–0.839) (Fig. 4D). We compared the predictive capabilities for prognosis using ROC curves for the nomogram score, DRLI, TNM staging, and ClearCode34 [reference]. Initially, we examined the prediction of 1-year prognosis, where the nomogram demonstrated remarkable predictive ability (AUC = 0.877), with DRLI also showing strong predictive power (AUC = 0.761), surpassing the predictive capability of TNM staging (T: AUC = 0.727; M: AUC = 0.719) (Fig. 4E). However, while TNM staging effectively reflects the cross-sectional status at diagnosis, its ability to predict long-term prognosis significantly decreases. In predicting 10-year prognosis, the AUC values for TNM staging did not exceed 0.7. In contrast, the AUC for DRLI reached 0.823, closely approaching the nomogram's AUC of 0.826. As time progresses, the predictive accuracy of DRLI becomes even more precise, indicating that our model effectively reflects the long-term prognosis of ccRCC.

3.4. Tumor microenvironment across DRLI subgroups

Preliminary single-cell studies [21] unveiled heterogeneity in the ccRCC microenvironment cell population based on established markers, encompassing non-classical monocytes (Mono_nc), natural killer T cells (NK_T), CD8 T cells (CD8T), B cells (B_cell), CD4 T cells (CD4T), ccRCC cells, classical monocytes (Mono_c), proximal tubular cells expressing GPX3 (PT_GPX3), epithelial cells (Epith),

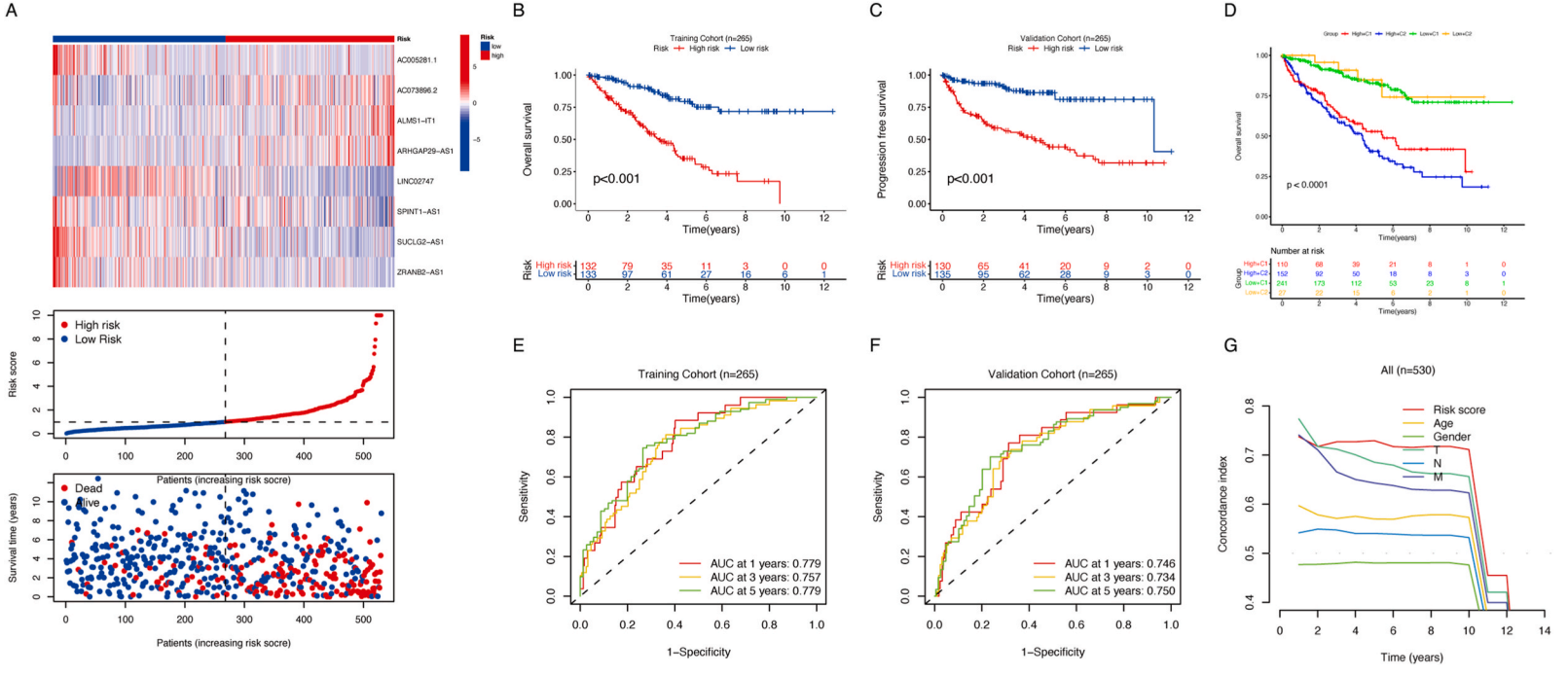

Fig. 3. A: Heatmap with expression of 8 key lncRNAs in TCGA-ccRCC cohort, alongside Risk Score and Survival Status plots based on DRLI stratification. B: Overall Survival Kaplan-Meier curve for ccRCC patients in the training set, categorized by DRLI. C: Progression-Free Survival Kaplan-Meier curves for the validation cohort, stratified by DRLI. D: Overall Survival Kaplan-Meier curves comparing DRLI stratification with disulfidoptosis gene subtypes. E–F: ROC curves for 1-year, 3-year, and 5-year survival predictions in training (E) and validation (F) cohorts based on DRLI. G: The concordance index (C-index) over time comparing the predictive accuracy of the Disulfidoptosis-Related lncRNA Index (DRLI) against traditional clinical parameters in the ccRCC patient cohort.

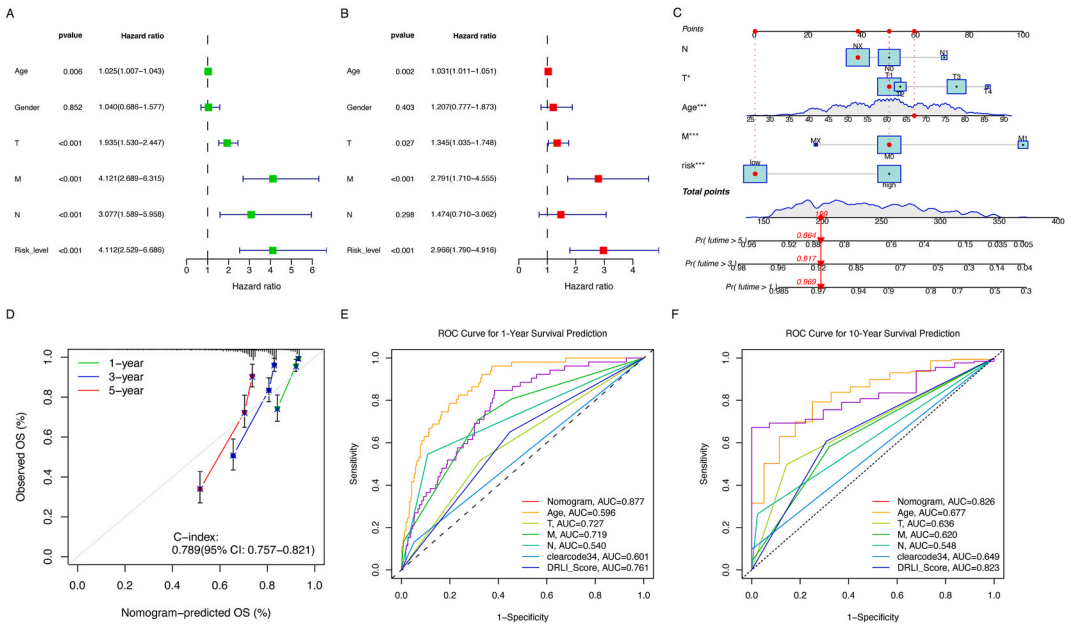

Fig. 4. A: Single-factor Cox regression analysis evaluating the impact of clinical factors and DRLI on ccRCC prognosis. B: Hazard ratio (HR) of DRLI and other clinical factors in multivariate Cox regression analysis. C: Nomogram integrating T stage, N stage, M stage, age, and DRLI for survival prediction in ccRCC patients. D: Calibration curve for the nomogram in the ccRCC cohort. E: ROC Curves Comparing 1-Year Prognostic Predictions. F: ROC Curves for 10-Year Prognostic Predictions.

proliferating cells (Prolif), plasma cells (PlasmaC), natural killer cells expressing CD160 (NK_CD160), proximal tubular cells expressing MT1G (PT_MT1G), neutrophils (Neutrop), natural killer cells (NK), endothelial cells (Endoth), conventional dendritic cells type 2 (cDC 2), mast cells (Mast), plasmacytoid dendritic cells (pDC), regulatory T cells (Treg), conventional dendritic cells type 1 (cDC 1), macrophages expressing C1QA (Mac_C1QA), and fibroblasts (Fibro), totaling 23 cell types (Fig. 5A). To further explore the immune status and prognostic landscape of the ccRCC microenvironment, we applied CIBERSORTx (https://cibersortx.stanford.edu/), implementing digital cytometry to deconvolute gene expression data into cell type abundances using a reference panel derived from scRNAseq. Initially, cell type-specific expression signatures were inferred from annotated ccRCC scRNA-seq datasets (GSE222703), identifying 1568 genes as specific markers. Subsequently, these feature genes were employed to enumerate the 23 cell types within the ccRCC microarray data. Significant enrichment of ccRCC cells, PT_GPX3, Endoth, and Fibro was observed within the tumor samples, exhibiting considerable intertumoral heterogeneity (Fig. 5B). The DRLI-high subgroup presented with a relatively higher presence of ccRCC and Fibro cells, while PT_GPX3 and Endoth cells were more prevalent in the DRLI-low subgroup. Further analysis of the infiltration of 22 immune cell types within the ccRCC cohort revealed statistically significant distribution differences between the two DRLI subgroups for 11 immune cell types, including Tregs (Fig. 5C). The influence of different tumor microenvironment cell abundances on the ccRCC cohort was calculated, indicating that Fibro, Macrophages M0, and T cells regulatory (Tregs) are predictive of poor outcomes in ccRCC patients. Higher infiltration of Dendritic cells resting, Endoth, Mast cells resting, and PT_GPX3 cells correlated with better ccRCC prognosis (Fig. 5D). Additionally, ESTIMATE was utilized to assess the tumor microenvironment score within the ccRCC cohort, with the immune score and estimate score being higher in the DRLI-high subgroup, suggesting greater immune infiltration in ccRCC with higher DRLI (Fig. 5E). The potential response to immune checkpoint therapy in the ccRCC cohort was evaluated using TIDE, indicating that the DRLI-high subgroup had higher TIDE scores than the DRLI-low subgroup, suggesting a likelihood of immune evasion and poor response to immune checkpoint therapy (Fig. 5F). Comparison of Tumor Mutation Burden (TMB) between the DRLI subgroups revealed no significant differences (Fig. 5G).

3.5. *Molecular characteristics of DRLI subgroups*

In our investigation, we conducted a principal component analysis (PCA) of the transcriptome to discern transcriptional disparities between the DRLI-high and DRLI-low subgroups in ccRCC. The PCA, executed using a script that processed expression data from a variety of sources, including genes and lncRNAs, displayed distinct clustering patterns, signaling significant transcriptional divergence between the two risk groups. These observations corroborate the potential utility of DRLI as a biomarker for ccRCC characterization and treatment stratification (Fig. 6A).

GSVA was employed to analyze the ccRCC cohort for hallmark pathways (Fig. 6B), revealing that several meaningful pathways were more activated in the DRLI-high group compared to the low group, such as TNFA signaling via NFkB, epithelial-mesenchymal transition, p53 pathway, IL6 JAK STAT3 signaling, and others.

Differential gene expression between the DRLI subgroups was identified using the 'limma' R package, revealing 344 genes

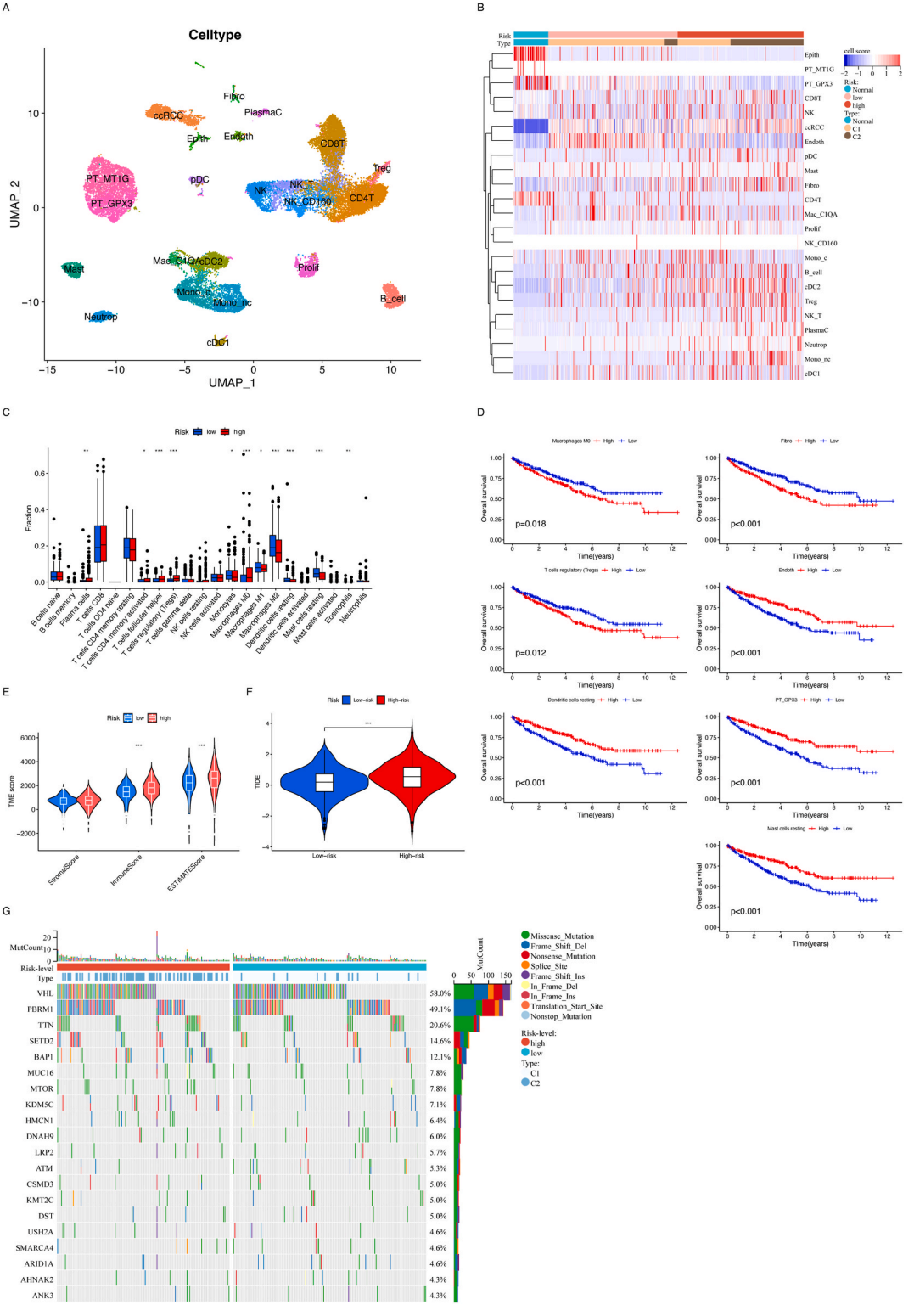

(caption on next page)

Fig. 5. A: Visualization of cell population heterogeneity in the ccRCC tumor microenvironment based on single-cell RNA sequencing data, categorizing cells into 23 types. B: Analysis of cell type distribution within ccRCC tumor samples, revealing significant variation in cell type abundance. C: Differential immune cell infiltration in DRLI subgroups, showing significant differences in 11 immune cell types between high and low DRLI groups. D: Kaplan-Meier survival curves correlating the prognostic impact of immune cell populations with patient outcomes in the ccRCC cohort. E: ESTIMATE scores within the ccRCC cohort, comparing immune and stromal scores between DRLI subgroups. F: TIDE analysis for ccRCC cohorts stratified by DRLI, predicting potential responses to immune checkpoint therapy. G： Waterfall plot of Tumor Mutation Burden (TMB) across the ccRCC cohort, detailing the mutational landscape relative to DRLI categorization.

upregulated in the DRLI-high subgroup and 105 downregulated genes (Fig. 6C). GO and KEGG pathway enrichment analyses were performed on these differentially expressed genes. The KEGG pathways primarily enriched included the IL-17 signaling pathway, Cytokine-cytokine receptor interaction, and PPAR signaling pathway (Fig. 6D). GO analysis predominantly highlighted enrichment in immune and inflammatory responses (Fig. 6E).

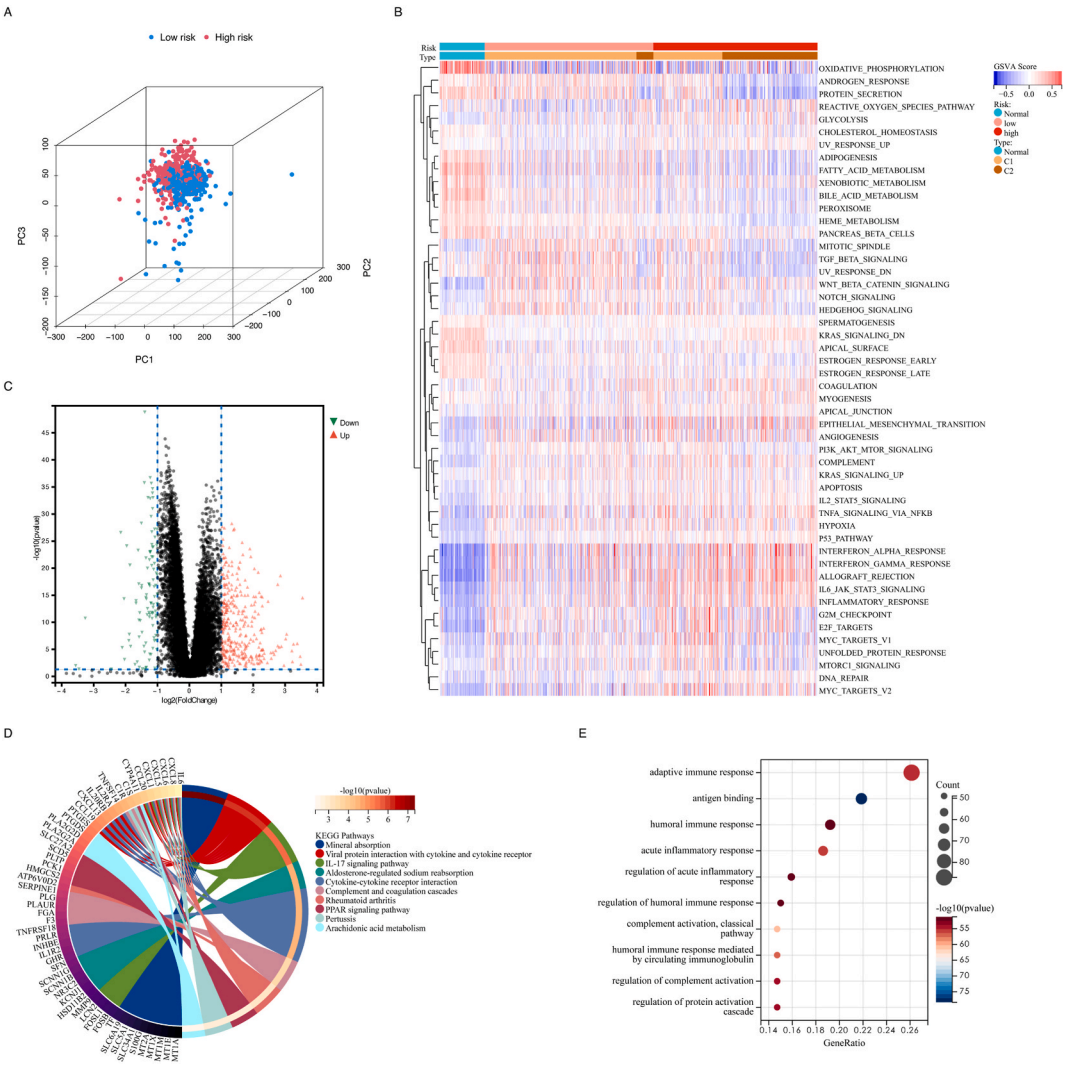

Fig. 6. A: Principal Component Analysis (PCA) displaying the divergence in transcriptional landscapes between the high and low DRLI-defined subgroups in the ccRCC transcriptome. B: Gene Set Variation Analysis (GSVA) illustrating differential pathway activations between high and low DRLI groups in the ccRCC cohort. C: Volcano plot of differentially expressed genes between DRLI subgroups; genes overexpressed in the DRLI-high group are marked in red, while those underexpressed are marked in green. D: KEGG pathway enrichment analysis of differentially expressed genes between DRLI subgroup E: GO analysis of genes differentially expressed between DRLI subgroups, elucidating their biological functions and associated processes. (For interpretation of the references to colour in this figure legend, the reader is referred to the Web version of this article.)

4. Discussion

Our study's development of the Disulfidoptosis-Related lncRNA Index (DRLI) represents a novel paradigm in the prognostication of clear cell renal cell carcinoma (ccRCC). The DRLI harnesses the prognostic power of lncRNAs associated with the oxidative stress pathway of disulfidoptosis, offering a more nuanced understanding of tumor biology and patient stratification.

The concept of disulfidoptosis, a form of cell death marked by disulfide stress [26], has been implicated in various malignancies but has not been thoroughly investigated in ccRCC. Our findings indicate a profound difference in survival outcomes between clusters defined by disulfidoptosis-related gene expression, with the k-means derived clusters C1 and C2 demonstrating distinct prognostic outcomes (Fig. 2A–B). The better prognosis associated with cluster C1 suggests that the expression profile of disulfidoptosis-related genes could be leveraged to identify patients with potentially less aggressive disease. The inclusion of 10 such genes in our analysis provides a focused yet comprehensive insight into the oxidative stress landscape of ccRCC, and their correlation with survival times suggests their utility as targets for future therapeutic interventions [27].

Long non-coding RNAs have emerged as key regulatory molecules in cancer [28–30]. In our study, we identified 174 lncRNAs that showed significant correlation with the disulfidoptosis gene set (Fig. 2C). The prognostic significance of these lncRNAs was underscored by their association with the overall survival of ccRCC patients, emphasizing their potential as biomarkers for this subtype of kidney cancer. The DRLI, leveraging these lncRNAs, demonstrated a discriminative ability to categorize patients into high and low-risk groups with significantly different survival outcomes ($P < 0.001$) (Fig. 3C). Such differentiation is critical for guiding clinical decision-making and tailoring patient-specific treatment regimens.

The single and multivariate Cox regression analyses underscored the individual impact of these factors on ccRCC prognosis, with DRLI demonstrating a particularly notable hazard ratio (HR) of 2.996 (95 % CI: 1.790–4.916) (Fig. 4B). This high HR highlights the substantial influence of DRLI in the disease progression and prognosis of ccRCC patients, asserting its vital role in the nomogram.

The predictive capabilities of the nomogram, as evaluated through ROC curves, revealed its exceptional performance in short-term (1-year) prognosis prediction, boasting an AUC of 0.877. This impressive accuracy demonstrates the nomogram's utility in clinical settings for immediate treatment strategy planning and patient counseling. In comparison, traditional TNM staging, while useful in reflecting the immediate clinical status of the disease, showed a diminished ability to predict long-term prognosis [31]. Its AUC values for 1-year prognosis, although substantial, were lower than that of the nomogram and DRLI (Fig. 4E).

A critical observation from our analysis is the increasing precision of DRLI in long-term prognosis prediction. While the TNM staging's predictive power wanes over time, with AUC values not exceeding 0.7 for 10-year prognosis, DRLI's AUC ascends to 0.823, nearly mirroring the nomogram's AUC of 0.826. This trend indicates that DRLI not only holds potential for immediate prognostication but also becomes increasingly reliable for predicting long-term outcomes. The capacity of DRLI to accurately reflect the long-term prognosis of ccRCC patients makes it a powerful tool in the armamentarium of clinicians managing this disease (Fig. 4F).

The predictive accuracy of our model, as demonstrated by the AUC values, surpasses that of the established Clearcode34 system [32]. Traditional prognostic frameworks for renal cell carcinoma, such as TNM staging and UISS((University of California, Los Angeles Integrated Staging System) scores [33], are largely dependent on clinical and pathological details. While TNM staging is a cornerstone of current cancer staging protocols, its reliance on non-biological metrics limits its ability to differentiate between non-invasive and more aggressive tumor forms. Similarly, the UISS score, though widely adopted, falls short in providing a comprehensive prognosis for the broad spectrum of renal cell carcinoma subtypes, as it is tailored to specific renal cancers. These systems, primarily predicated on post-surgical staging and tumor grading, do not incorporate the molecular markers of kidney cancer which are pivotal for a thorough prognostic analysis.

In contrast to the gene-centric RCClnc4 [34] and Clearcode34, which primarily use genetic predictors but omit critical clinical information, our model acknowledges the significance of incorporating both genetic and clinical data for a full-bodied prognosis of renal cell carcinoma. It is this integration of multifaceted diagnostic elements that sets our approach apart, offering a more complete and nuanced assessment of patient outcomes.

The application of single-cell deconvolution techniques in our study has unveiled a complex portrait of the ccRCC microenvironment [35]. By analyzing the expression data from thousands of individual cells, we observed significant heterogeneity within the tumor microenvironment, characterized by varying abundances of specific cell types such as fibroblasts and endothelial cells (Fig. 5B). The relevance of these findings is further supported by the differential distribution of immune cell types like Tregs between the DRLI subgroups (Fig. 5C), hinting at a potential immunosuppressive milieu in higher-risk patients. This granularity of data provides a foundation for developing immunotherapeutic strategies tailored to the unique cellular composition of each tumor.

The immune microenvironment of ccRCC, particularly in relation to immune checkpoint blockade, has become a focal point of cancer research. Our use of the TIDE algorithm to predict potential responses to immunotherapy revealed that higher DRLI scores, associated with worse prognosis, might also indicate a propensity for immune evasion (Fig. 5F). This raises important considerations for the use of immunotherapies in ccRCC, as patients with high DRLI scores may require combination therapies or novel immunomodulatory strategies to overcome this evasion.

The transcriptional profiling conducted through principal component analysis (PCA) distinguished the DRLI subgroups with notable clarity, suggesting that the transcriptional divergence is reflective of underlying biological processes that could be exploited for therapeutic targeting (Fig. 6A). The activation of pathways such as TNFα signaling via NFκB and epithelial-mesenchymal transition in the high DRLI group (Fig. 6B) not only informs the aggressive nature of these tumors but also identifies potential molecular targets for drug development.

The clinical integration of our findings, particularly the DRLI and associated molecular signatures, promises to enhance the precision of prognostication and therapy selection in ccRCC. The validation of these markers in clinical settings remains a priority, with

potential implications for screening, monitoring, and therapeutic intervention. Our study's findings must be considered within the broader context of ongoing research into the genomics of cancer, where such indices could be combined with other molecular and imaging biomarkers for a more comprehensive prognostic model.

The innovative core of this study lies in the novel integration of disulfidoptosis-associated lncRNAs with the prognostic modeling of clear cell renal cell carcinoma (ccRCC). The Disulfidoptosis-Related lncRNA Index (DRLI) is a pioneering tool that combines the specificity of genetic expression with the functional implications of cell death pathways, providing a predictive accuracy that surpasses traditional clinical parameters. The stratification of ccRCC patients using the DRLI offers a glimpse into the heterogeneity of tumor behavior and its response to oxidative stress, suggesting potential personalized therapeutic avenues. In light of our findings, there lies an opportunity to investigate the synergistic effects of targeting disulfidoptosis pathways in conjunction with established treatment protocols. The robust correlation between DRLI and patient outcomes may reflect an underlying biological cascade that can be harnessed to enhance therapeutic efficacy. For instance, the exploration of drugs that modulate oxidative stress or amend lncRNA expression could yield novel combinations that potentiate the anti-tumor response in high DRLI score patients. Our study's approach underscores the value of integrating molecular diagnostics with clinical prognostication, advocating for a more dynamic treatment strategy that adapts to the molecular profile of the tumor. Future investigations should also delve into the potential crosstalk between disulfidoptosis and other cell death pathways, unraveling the complexity of ccRCC's pathophysiology and its implications for resistance or sensitivity to specific treatments. These efforts are essential in advancing the frontier of precision medicine and offering ccRCC patients a beacon of tailored therapeutic hope.

Despite these advancements, the study has limitations that need to be acknowledged. The reliance on retrospective TCGA data, while robust, cannot substitute the insights gained from a prospective study design. As with any bioinformatics approach, the conclusions drawn from computational models must be validated experimentally. The functional roles of the identified lncRNAs in disulfidoptosis and their impact on the immune microenvironment remain to be elucidated through in vitro and in vivo studies. Moreover, the prognostic applicability of the DRLI needs to be tested across diverse patient populations, with varying disease stages and treatment backgrounds, to fully understand its utility and limitations. Lastly, while the study breaks ground in the intersection of disulfidoptosis and lncRNAs, the clinical translation of these findings into actionable therapeutic strategies will require a concerted effort and poses a significant challenge for future research.

In conclusion, our study contributes a novel and clinically relevant prognostic model that could significantly influence the management of ccRCC. The DRLI and the insights gained from our extensive single-cell and molecular analyses provide a deeper understanding of ccRCC pathophysiology and lay the groundwork for personalized patient care. Future research should aim to translate these biomarkers into therapeutic targets and validate their utility in prospective clinical trials, with the ultimate goal of improving patient outcomes in ccRCC.

Ethics approval and consent to participate

The data used in this study were exclusively sourced from publicly available databases. These datasets do not contain any identifiable personal information. Consequently, the nature of this research precludes the necessity for ethics approval and individual consent.

Consent for publication

Not applicable.

Data availability

The datasets analyzed during the current study are available in the following repositories: The Cancer Genome Atlas (TCGA) which can be accessed at [https://portal.gdc.cancer.gov/], and the Gene Expression Omnibus (GEO) repository, with the specific dataset identifier GSE222703, accessible at [https://www.ncbi.nlm.nih.gov/geo/query/acc.cgi?acc=GSE222703].

Funding

This work was supported by the National Natural Science Foundation of China (82272834), the Special Fund of Taishan Scholars Project of Shandong Province, China (tsqn202306348), and the Natural Science Foundation of Shandong Province (ZR202306020045).

CRediT authorship contribution statement

Renhui Guan: Writing – review & editing, Writing – original draft, Methodology, Data curation. **You Zuo:** Visualization. **Qinglong Du:** Data curation. **Aijing Zhang:** Methodology. **Yijian Wu:** Methodology. **Jianguo Zheng:** Methodology. **Tongrui Shi:** Formal analysis. **Lin Wang:** Data curation. **Hui Wang:** Writing – review & editing, Writing – original draft, Supervision, Conceptualization. **Nengwang Yu:** Writing – review & editing, Writing – original draft, Conceptualization.

Declaration of competing interest

Nengwang Yu reports financial support provided by the National Natural Science Foundation of China (82272834), the Special Fund of Taishan Scholars Project of Shandong Province, China (tsqn202306348), and the Natural Science Foundation of Shandong Province (ZR202306020045). The other authors declare that they have no known competing financial interests or personal relationships that could have appeared to influence the work reported in this paper.

References

[1] F. Bray, J. Ferlay, I. Soerjomataram, R.L. Siegel, L.A. Torre, A. Jemal, Global cancer statistics 2018: GLOBOCAN estimates of incidence and mortality worldwide for 36 cancers in 185 countries, CA A Cancer J. Clin. 68 (6) (2018) 394–424.
[2] H. Wunderlich, S. Schumann, V. Jantitzky, P. Moravek, M. Podhola, H. Kosmehl, et al., Increase of renal cell carcinoma incidence in central Europe, Eur. Urol. 33 (6) (1998) 538–541.
[3] S. Brookman-May, M. May, S.F. Shariat, R. Zigeuner, T. Chromecki, L. Cindolo, et al., Prognostic effect of sarcomatoid dedifferentiation in patients with surgically treated renal cell carcinoma: a matched-pair analysis, Clin. Genitourin. Cancer 11 (4) (2013) 465–470.
[4] I. Lucca, M. de Martino, S.L. Hofbauer, N. Zamani, S.F. Shariat, T. Klatte, Comparison of the prognostic value of pretreatment measurements of systemic inflammatory response in patients undergoing curative resection of clear cell renal cell carcinoma, World J. Urol. 33 (12) (2015) 2045–2052.
[5] S.B. Edge, C.C. Compton, The American Joint Committee on Cancer: the 7th edition of the AJCC cancer staging manual and the future of TNM, Ann. Surg Oncol. 17 (6) (2010) 1471–1474.
[6] H. Moch, W. Artibani, B. Delahunt, V. Ficarra, R. Knuechel, F. Montorsi, et al., Reassessing the current UICC/AJCC TNM staging for renal cell carcinoma, Eur. Urol. 56 (4) (2009) 636–643.
[7] I. Frank, M.L. Blute, J.C. Cheville, C.M. Lohse, A.L. Weaver, H. Zincke, An outcome prediction model for patients with clear cell renal cell carcinoma treated with radical nephrectomy based on tumor stage, size, grade and necrosis: the SSIGN score, J. Urol. 168 (6) (2002) 2395–2400.
[8] W.P. Parker, J.C. Cheville, I. Frank, H.B. Zaid, C.M. Lohse, S.A. Boorjian, et al., Application of the stage, size, grade, and necrosis (SSIGN) score for clear cell renal cell carcinoma in contemporary patients, Eur. Urol. 71 (4) (2017) 665–673.
[9] J. Mischinger, E. Fröhlich, S. Mannweiler, C. Meindl, M. Absenger-Novak, G.C. Hutterer, et al., Prognostic value of B7-H1, B7-H3 and the stage, size, grade and necrosis (SSIGN) score in metastatic clear cell renal cell carcinoma, Cent European J Urol 72 (1) (2019) 23–31.
[10] X. Liu, L. Nie, Y. Zhang, Y. Yan, C. Wang, M. Colic, et al., Actin cytoskeleton vulnerability to disulfide stress mediates disulfidptosis, Nat. Cell Biol. 25 (3) (2023) 404–414.
[11] X. Liu, K. Olszewski, Y. Zhang, E.W. Lim, J. Shi, X. Zhang, et al., Cystine transporter regulation of pentose phosphate pathway dependency and disulfide stress exposes a targetable metabolic vulnerability in cancer, Nat. Cell Biol. 22 (4) (2020) 476–486.
[12] D. Zhang, X. Zhang, Z. Liu, T. Han, K. Zhao, X. Xu, et al., An integrative multi-omics analysis based on disulfidptosis-related prognostic signature and distinct subtypes of clear cell renal cell carcinoma, Front. Oncol. 13 (2023) 1207068.
[13] T. Chu, Z. Wang, D. Pe'er, C.G. Danko, Cell type and gene expression deconvolution with BayesPrism enables Bayesian integrative analysis across bulk and single-cell RNA sequencing in oncology, Nat. Can. (Ott.) 3 (4) (2022) 505–517.
[14] A.M. Newman, C.L. Liu, M.R. Green, A.J. Gentles, W. Feng, Y. Xu, et al., Robust enumeration of cell subsets from tissue expression profiles, Nat. Methods 12 (5) (2015) 453–457.
[15] C.U. Monjaras-Avila, A.C. Lorenzo-Leal, A.C. Luque-Badillo, N. D'Costa, C. Chavez-Muñoz, H. Bach, The tumor immune microenvironment in clear cell renal cell carcinoma, Int. J. Mol. Sci. 24 (9) (2023).
[16] A. Colaprico, T.C. Silva, C. Olsen, L. Garofano, C. Cava, D. Garolini, et al., TCGAbiolinks: an R/Bioconductor package for integrative analysis of TCGA data, Nucleic Acids Res. 44 (8) (2016) e71.
[17] M. Mounir, M. Lucchetta, T.C. Silva, C. Olsen, G. Bontempi, X. Chen, et al., New functionalities in the TCGAbiolinks package for the study and integration of cancer data from GDC and GTEx, PLoS Comput. Biol. 15 (3) (2019) e1006701.
[18] A. Frankish, M. Diekhans, I. Jungreis, J. Lagarde, E. Loveland Jane, J.M. Mudge, et al., Gencode 2021, Nucleic Acids Res. 49 (D1) (2020) D916–D923.
[19] S. Hänzelmann, R. Castelo, J. Guinney, GSVA: gene set variation analysis for microarray and RNA-seq data, BMC Bioinf. 14 (2013) 7.
[20] A. Liberzon, C. Birger, H. Thorvaldsdóttir, M. Ghandi, J.P. Mesirov, P. Tamayo, The Molecular Signatures Database (MSigDB) hallmark gene set collection, Cell Syst 1 (6) (2015) 417–425.
[21] L. Massenet-Regad, J. Poirot, M. Jackson, C. Hoffmann, E. Amblard, F. Onodi, et al., Large-scale analysis of cell-cell communication reveals angiogenin-dependent tumor progression in clear cell renal cell carcinoma, iScience 26 (12) (2023) 108367.
[22] L. McInnes, J. Healy, J. Melville, UMAP: Uniform Manifold approximation and projection for dimension reduction, arXiv (2020).
[23] K. Yoshihara, M. Shahmoradgoli, E. Martínez, R. Vegesna, H. Kim, W. Torres-Garcia, et al., Inferring tumour purity and stromal and immune cell admixture from expression data, Nat. Commun. 4 (2013) 2612.
[24] J. Fu, K. Li, W. Zhang, C. Wan, J. Zhang, P. Jiang, et al., Large-scale public data reuse to model immunotherapy response and resistance, Genome Med. 12 (1) (2020) 21.
[25] P. Jiang, S. Gu, D. Pan, J. Fu, A. Sahu, X. Hu, et al., Signatures of T cell dysfunction and exclusion predict cancer immunotherapy response, Nat. Med. 24 (10) (2018) 1550–1558.
[26] D. He, H. Tang, X. Yang, X. Liu, Y. Zhang, J. Shi, Elaboration and validation of a prognostic signature associated with disulfidoptosis in lung adenocarcinoma, consolidated with integration of single-cell RNA sequencing and bulk RNA sequencing techniques, Front. Immunol. 14 (2023) 1278496.
[27] S. Ma, Y. Ge, Z. Xiong, Y. Wang, L. Li, Z. Chao, et al., A novel gene signature related to oxidative stress predicts the prognosis in clear cell renal cell carcinoma, PeerJ 11 (2023) e14784.
[28] W.H. Yu, C.L. Hsu, C.C. Lin, Y.J. Oyang, H.F. Juan, H.C. Huang, Stratification of lncRNA modulation networks in breast cancer, BMC Med. Genom. 14 (Suppl 3) (2022) 300.
[29] M. Ma, J. Li, Z. Zeng, Z. Zheng, W. Kang, Integrated analysis from multicentre studies identities m7G-related lncRNA-derived molecular subtypes and risk stratification systems for gastric cancer, Front. Immunol. 14 (2023) 1096488.
[30] Z. Zhang, Z. Xu, Y. Yan, Role of a pyroptosis-related lncRNA signature in risk stratification and immunotherapy of ovarian cancer, Front. Med. 8 (2021) 793515.
[31] G.P. Paner, W.M. Stadler, D.E. Hansel, R. Montironi, D.W. Lin, M.B. Amin, Updates in the eighth edition of the tumor-node-metastasis staging classification for urologic cancers, Eur. Urol. 73 (4) (2018) 560–569.
[32] P. Ghatalia, W.K. Rathmell, Systematic review: ClearCode 34 - a validated prognostic signature in clear cell renal cell carcinoma (ccRCC), Kidney Cancer 2 (1) (2018) 23–29.
[33] R. Zigeuner, G. Hutterer, T. Chromecki, A. Imamovic, K. Kampel-Kettner, P. Rehak, et al., External validation of the Mayo Clinic stage, size, grade, and necrosis (SSIGN) score for clear-cell renal cell carcinoma in a single European centre applying routine pathology, Eur. Urol. 57 (1) (2010) 102–109.
[34] L. Qu, Z.L. Wang, Q. Chen, Y.M. Li, H.W. He, J.J. Hsieh, et al., Prognostic value of a long non-coding RNA signature in localized clear cell renal cell carcinoma, Eur. Urol. 74 (6) (2018) 756–763.
[35] M. Kuksin, D. Morel, M. Aglave, F.X. Danlos, A. Marabelle, A. Zinovyev, et al., Applications of single-cell and bulk RNA sequencing in onco-immunology, Eur. J. Cancer 149 (2021) 193–210.